Electricity Flexibility Evaluation of Hydrogen-Based Steelmaking with Solar PV Electrolysis

Zhuo Chen, Manjun Chen, Xiandong Xu, Hongjie Jia
State key laboratory of Smart Power Distribution Equipment and System
Tianjin University
Tianjin, China
zhuochen@tju.edu.cn, cmj416@tju.edu.cn, xux27@tju.edu.cn, hjjia@tju.edu.cn

***Abstract*—Hydrogen-based direct reduced iron (DRI) short-process steelmaking is a pathway for decarbonization and an important source of grid flexibility. Solar photovoltaic (PV)-driven anion-exchange membrane (AEM) co-electrolysis converts fluctuating PV output into storable H_2 and CO, which can be used as reducing gas and gaseous fuel in hydrogen-based short-process steelmaking. However, the integrated operation and plant-level flexibility of PV-driven co-electrolysis integrated (PV-EC-integrated) hydrogen-based DRI short-process steel plants have not yet been investigated. A batch-oriented resource-task network (RTN) model is developed for such an integrated plant. On this basis, a plant-level flexibility evaluation method is formulated to characterize deliverable peak-shaving and valley-filling capacities for different signal start times and service durations. Numerical results show that PV-driven H_2/CO production shapes feasible production schedules, while H_2/CO storage mitigates temporal mismatches between PV power output and steelmaking demand and thereby supports flexibility provision. The resulting flexibility depends on both the signal start time and the service duration.**

***Keywords*—Flexibility, short-process steelmaking, solar PV electrolysis, syngas**

I. Introduction

With the accelerated global efforts to reduce carbon emissions, the power grid is undergoing a profound transformation to integrate renewable energy [1]. This transformation results in higher demand for flexibility in balancing power supply and demand [2]. Hereby flexibility can be defined as "the potential for modification of appliance power profile by adjusting power draw, the operation duration, and/or the activation time" [3].

As a fundamental pillar of modern industry, steel production deserves particular attention as a source of flexibility. In particular, hydrogen-based short-process steelmaking is considered to achieve lower carbon emissions and greater operational flexibility than conventional long-route steelmaking [4]. The provision of this flexibility relies on the coordination of different procedures, such as electric arc furnace (EAF), ladle furnace (LF), continuous casting (CC) and hot rolling (HR).

Solar photovoltaic-driven CO_2/H_2O co-electrolysis systems (PV-EC systems) converts fluctuating PV output into storable H_2/CO syngas [5]. When coupled with hydrogen-based short-process steelmaking, PV-EC system can turn renewable electricity into process gases which in principle helps mitigate renewable-generation variability and offers additional demand-side flexibility.

Short-process steelmaking operates in discrete heats with sequential transfers (EAF→LF→CC→HR) [6]. Beyond batch scheduling, both the EAF and the LF employ on-load tap changers (OLTCs), enabling adjustable load profiles during operation [7]. Building on this batch-oriented production, a short-process steelmaking model based on the RTN is developed in [8] to examine the impact of time-varying electricity prices on production scheduling. The OLTC-enabled load adjustability of the EAF is explicitly embedded in an RTN framework in [9], broadening flexibility studies for short-process plants. LF flexibility is further represented in the RTN formulation of the AOD-LF-CC route in [10]. Its thermal inertia is modeled to assess downward-regulation durations in [11]. To improve tractability, a two-stage solution approach is proposed in [12]. In addition, DRI-EAF production is coupled with the operation of a proton-exchange-membrane (PEM) water electrolyzer supplying hydrogen to the DRI shaft furnace in [13], highlighting the interaction between power-to-hydrogen systems and steelmaking. To the authors' best knowledge, no prior work has explicitly modeled PV-EC-integrated hydrogen-based short-process steel plants and analyzed their plant-level flexibility.

Motivated by this gap, this paper develops a model-based plant-level flexibility evaluation method for PV-EC-integrated hydrogen-based short-process steel plants. A batch-oriented RTN model is formulated to represent the coupled material-energy flows, storage states, and batch operations on a unified time grid. Based on this model, the proposed method quantifies plant-level peak-shaving and valley-filling capacities over different signal start times and service durations.

II. Modelling of Hydrogen-Based Steel Production Driven by Solar PV Panels

A. System Description

Fig. 1 depicts a PV-EC-integrated hydrogen-based short-process steel plant. PV powers an AEM co-electrolyzer that co-produces H_2 and CO, which are separated downstream. H_2 feeds the DRI shaft furnace either directly or via H_2 storage, while CO is stored and later used as an auxiliary gaseous fuel in the EAF and HR. The shaft furnace produces DRI, which transfer cars deliver to the EAF for primary melting, then to the LF for secondary refining and CC for casting, where the ladle turret provides a single-ladle buffer. Cast slabs are hot-charged to HR to obtain finished products. The plant remains grid-connected for electric power.

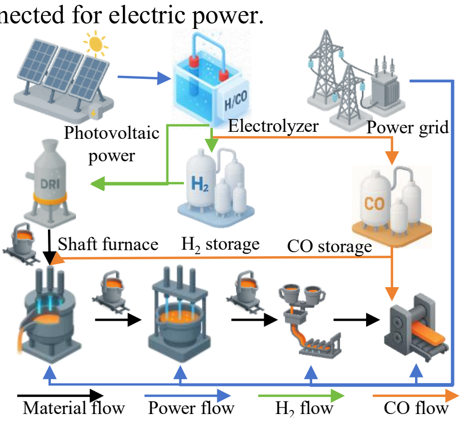

Fig. 1. PV-EC-integrated hydrogen-DRI short-process steel plant.

This work is supported by National Key R&D Program of China (2023YFB2407300).
979-8-3315-8138-1

To unify the temporal representation of equipment and materials, the RTN resource balance is adopted. A resource's stock evolves with the discrete (start/end) and continuous (production/consumption) interactions of tasks, which is expressed as

$$R_{r,t} = R_{r,t-1} + \sum_{i\in\mathcal{I}_r}\sum_{\theta=0}^{\tau_i}(\mu_{r,i,\theta}\bullet N_{i,t-\theta} + \nu_{r,i,\theta}\bullet\xi_{i,t-\theta}) + \prod\nolimits_{r,t} \quad (1)$$

where $R_{r,t}$ represents the availability of resource r at time slot t. $\mathcal{I}_r$ represents the tasks that interact with r. $N_{i,t-\theta}$ is a 0-1 variable, with a value of 1 indicating that t

he discrete event task i at time t. $\xi_{i,t}$ represents the continuous rate of task i at time t. τ_i represents the memory horizon of task i. $\mu_{i,r,\theta}$ represents the discrete coupling coefficient. $\nu_{r,i,\theta}$ represents the continuous coupling coefficient. $\prod_{r,t}$ represents the exogenous flow. As an example, Fig. 2 illustrates the RTN formulation for the EAF melting task.

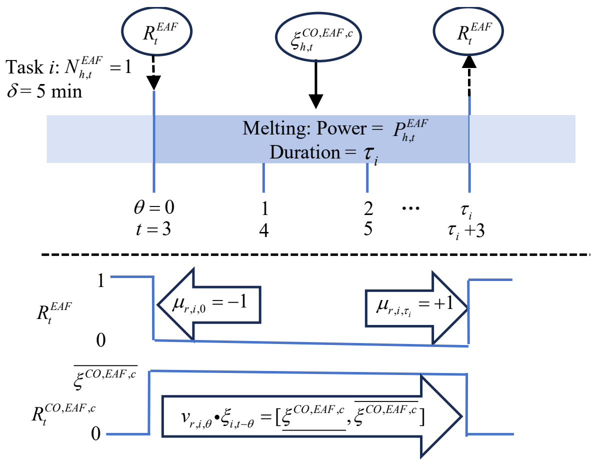

Fig. 2. Illustration of interaction parameters for EAF task.

B. Task Execution

Task execution is organized into two categories.

1) Slot-activatable flow tasks, where a binary decision in each time slot switches a continuous rate on or off (e.g., charging/discharging of H_2).

2) Batch-production tasks, where each batch remains in process for a contiguous sequence of slots (e.g., EAF and LF heats).

The charging/discharging rate of the H_2 storage is gated by a binary activation decision and bounded by the capacity limits in each time slot: the rate is zero when inactive and lies within the prescribed bounds when active, which is expressed as

$$N_t^{H_2,i}\bullet\underline{\xi^{H_2,i}} \le \xi_t^{H_2,i} \le \overline{\xi^{H_2,i}}\bullet N_t^{H_2,i} \quad \forall i\in\{dis,ch\} \quad (2)$$

where $N_t^{H_2,dis}$ and $N_t^{H_2,ch}$ are 0-1 variables, with a value of 1 indicating that the H_2 storage is discharging or charging at time t, respectively. $\xi_t^{H_2,dis}$ and $\xi_t^{H_2,ch}$ represent the H_2 discharging and charging flow rates at time t, respectively. $\underline{\xi^{H_2,dis}}$ and $\overline{\xi^{H_2,dis}}$ represent the lower and upper bounds of the H_2-storage discharging rate. $\underline{\xi^{H_2,ch}}$ and $\overline{\xi^{H_2,ch}}$ represent the lower and upper bounds of the charging rate, respectively.

Due to the process characteristics of the H_2 storage, charging and discharging are mutually exclusive in any time slot; at most one can be active at a time, which is expressed as

$$N_t^{H_2,dis} + N_t^{H_2,ch} \le 1 \quad (3)$$

Unlike the H_2 tank, the CO gasholder is a buffer that can receive and deliver simultaneously. When heat h is in process at time t, the CO outflow to the EAF must lie within the capacity band; otherwise it is forced to zero, which is expressed as

$$S_{h,t}^{EAF}\bullet\underline{\xi^{CO,EAF,c}} \le \xi_{h,t}^{CO,EAF,c} \le \overline{\xi^{CO,EAF,c}}\bullet S_{h,t}^{EAF} \quad (4)$$

where $S_{h,t}^{EAF}$ is a 0-1 variable, with a value of 1 indicating that EAF heat h is in process at time t. $\xi_{h,t}^{CO,EAF,c}$ represents the CO delivery rate to the EAF for heat h at time t. $\underline{\xi^{CO,EAF,c}}$ and $\overline{\xi^{CO,EAF,c}}$ represent the lower and upper bounds of the CO delivery rate to the EAF, respectively.

H_2 consumption by the DRI shaft furnace, the DRI production rate, and CO consumption by hot rolling are modeled as fixed-rate processes. When a task is in process, its rate equals a constant, which is expressed as

$$\xi_t^{H_2,DRI,c} = V_{fix}^{H_2,DRI,c}\bullet N_t^{DRI} \quad (5)$$

$$\xi_t^{DRI,p} = V_{fix}^{DRI,p}\bullet N_t^{DRI} \quad (6)$$

$$\xi_{h,t}^{CO,HR,c} = V_{fix}^{CO,HR,c}\bullet S_{h,t}^{HR} \quad (7)$$

where $\xi_t^{H_2,DRI,c}$ represents the H_2 consumption by the DRI shaft furnace at time t. $\xi_t^{DRI,p}$ represents the DRI production rate at time t. $\xi_{h,t}^{CO,HR,c}$ represents the CO consumption rate of hot rolling for heat h at time t. $V_{fix}^{H_2,DRI,c}$, $V_{fix}^{DRI,p}$ and $V_{fix}^{CO,HR,c}$ represent the fixed rates of H_2 consumption by shaft furnace, DRI production, and CO consumption by hot rolling, respectively. N_t^{DRI} is a 0-1 variable, with a value of 1 indicating that shaft furnace starts at time t. $S_{h,t}^{HR}$ is a 0-1 variable, with a value of 1 indicating that HR heat h is in process at time t.

Batch production is characterized using an event-state difference formulation, in which start and end events are coupled with the in-process state. Consequently, each heat is represented by a single contiguous in-process interval (state = 1) on the time axis, which is expressed as

$$S_{h,t}^{i} - S_{h,t-1}^{i} = N_{h,t}^{i} - N_{h,t}^{ie}$$

$$\forall i\in\{EAF/LF/CC,arr/CC/HR\} \quad (8)$$

$$\forall ie\in\{EAF,end/LF,end/CC/CC,end/HR,end\}$$

where $N_{h,t}^{EAF}$, $N_{h,t}^{LF}$, $N_{h,t}^{CC,arr}$, $N_{h,t}^{CC}$ and $N_{h,t}^{HR}$ are 0-1 variables, with a value of 1 indicating that represent the start of EAF, the start of LF, the arrival of the ladle at the ladle turret of CC, the start of CC, and the start of HR for heat h at time t, respectively. $N_{h,t}^{EAF,end}$, $N_{h,t}^{LF,end}$, $N_{h,t}^{CC,end}$ and $N_{h,t}^{HR,end}$ represent the completion of the EAF heat, the completion of the LF heat, the completion of CC, and the completion of HR for heat h at time t, respectively. $S_{h,t}^{LF}$, $S_{h,t}^{CC,arr}$, $S_{h,t}^{CC}$ and $S_{h,t}^{HR}$ are 0-1 variables, with a value of 1 indicating, respectively, that LF heat h is in process, the ladle of heat h occupies the ladle turret of CC (arrival buffer), CC heat h is in process, and HR heat h is in process at time t.

Each batch production task starts exactly once over the time horizon, which is expressed as

$$\sum_{t\in\mathcal{T}} N_{h,t}^{i} = 1 \;\forall i \in \{DRI,Tr / EAF / LF / CC,arr / CC / HR\} \quad (9)$$

where $N_{h,t}^{DRI,Tr}$ is a 0-1 variable, with a value of 1 indicating that the start of the DRI→EAF transfer for heat *h* at time *t*.

C. Resource Balance

The balances for equipment and material resources are formulated differently to reflect the production characteristics of each process. Accordingly, the following equations formalize the discrete-time balances for material stocks and transfer-car occupancy.

The H_2 consumed by the shaft furnace is supplied from two sources: H_2 released from storage and H_2 delivered directly from the electrolyzer to the DRI, which is expressed as

$$\xi_t^{H_2,DRI,c} = \xi_t^{H_2,DRI} + \xi_t^{H_2,dis} \quad (10)$$

where $\xi_t^{H_2,DRI}$ represents the H_2 flow rate delivered directly to the DRI at time *t*.

The H_2 produced by the PV-EC system is split between two destinations: delivery to the shaft furnace and charging of the H_2 storage. And the CO produced by the PV-EC system is in a fixed proportion to its H_2 output, which is expressed as

$$\prod\nolimits_t^{H_2} = \xi_t^{H_2,DRI} + \xi_t^{H_2,ch} = K^{H_2/CO} \bullet \prod\nolimits_t^{CO} \quad (11)$$

where $\prod_t^{H_2}$ represents the H_2 produced by the PV-EC system at time *t*. $\prod_t^{CO}$ represents the CO produced by the PV-EC system at time *t*. $K^{H_2/CO}$ represents the constant yield ratio.

The H_2 storage level is governed by charging and discharging, which is expressed as

$$R_t^{H_2,sto} = R_{t-1}^{H_2,sto} + \xi_t^{H_2,ch} - \xi_t^{H_2,dis} \quad (12)$$

where $R_t^{H_2,sto}$ represents the H_2 storage level at time *t*.

The CO storage is replenished by the PV-EC system and is depleted when the EAF and HR are in operation, which is expressed as

$$R_t^{CO,sto} = R_{t-1}^{CO,sto} - \sum_{h\in\mathcal{H}} \xi_{h,t}^{CO,EAF,c} - \sum_{h\in\mathcal{H}} \xi_{h,t}^{CO,HR,c} + \prod\nolimits_t^{CO} \quad (13)$$

where $R_t^{CO,sto}$ represents the CO storage level at time *t*.

The DRI production is continuous while the shaft furnace is in operation, whereas withdrawals occur as discrete per-heat transfers triggered by transfer-car start events, which is expressed as

$$R_t^{DRI,sto} = R_{t-1}^{DRI,sto} + \xi_t^{DRI,p} - \mu_{fix}^{DRI} \bullet \sum_{h\in\mathcal{H}} N_{h,t}^{DRI,Tr} \quad (14)$$

where $R_t^{DRI,sto}$ represents the DRI storage level at time *t*. μ_{fix}^{DRI} represents the fixed DRI quantity transferred per heat.

For the DRI→EAF and EAF→LF processes, the transfer car may wait at the downstream station before the next process begins; once the start event occurs, the car departs and remains occupied during the return, and is released only after the return is completed, which is expressed as

$$R_t^{DRI,Car} = R_{t-1}^{DRI,Car} - \sum_{h\in\mathcal{H}} N_{h,t}^{DRI,Tr} + \sum_{h\in\mathcal{H}} N_{h,t-tr_{back}}^{EAF} \quad (15)$$

$$R_t^{EAF,Car} = R_{t-1}^{EAF,Car} - \sum_{h\in\mathcal{H}} N_{h,t}^{EAF,end} + \sum_{h\in\mathcal{H}} N_{h,t-tr_{back}}^{LF} \quad (16)$$

where $R_t^{DRI,Car}$ and $R_t^{EAF,Car}$ represent the transfer cars for the DRI→EAF and EAF→LF transfers, respectively.

Unlike the preceding transfers, in the LF→CC transfer the car places the ladle on the caster's ladle turret (arrival buffer) and departs immediately; it remains occupied during the return and is released only when the return is completed, which is expressed as

$$R_t^{LF,Car} = R_{t-1}^{LF,Car} - \sum_{h\in\mathcal{H}} N_{h,t}^{LF,end} + \sum_{h\in\mathcal{H}} N_{h,t-tr_{back}}^{CC,arr} \quad (17)$$

where $R_t^{LF,Car}$ represents the transfer cars for the LF→CC transfer.

D. Transfer Time

During the DRI→EAF and EAF→LF transfers, the transfer car may incur a controllable delay at the downstream station before the next process begins, which is expressed as

$$T_h^{EAF,beg} = T_h^{DRI,Tr,beg} + T_{fix}^{DRI,Tr} + T_h^{DRI,Tr,dly} \quad (18)$$

$$T_h^{LF,beg} = T_h^{EAF,end} + T_{fix}^{EAF,Tr} + T_h^{EAF,Tr,dly} \quad (19)$$

For the LF→CC transfer, the travel time to the caster is fixed; upon arrival, the ladle waits on the ladle turret with a controllable delay until CC starts, which is expressed as

$$T_h^{CC,arr} = T_h^{LF,end} + T_{fix}^{LF,Tr} \quad (20)$$

$$T_h^{CC,beg} = T_h^{CC,arr} + T_h^{CC,dly} \quad (21)$$

In CC, heats within the same casting sequence must run back-to-back without gaps, whereas between sequences a sufficient tundish-changeover interval must be reserved, which is expressed as

$$\text{if } h \bmod n^{cast} \neq 0,\; T_{h+1}^{CC,beg} = T_h^{CC,end} \quad (22)$$

$$\text{if } h \bmod n^{cast} = 0,\; T_{h+1}^{CC,beg} \geq T_h^{CC,end} + T_{fix}^{chg} \quad (23)$$

Because HR is direct hot charging, the CC→HR transfer time is fixed, which is expressed as

$$T_h^{HR,beg} = T_h^{CC,end} + T_{fix}^{CC,Tr} \quad (24)$$

The start and end times of batch task are given by time-weighted sums of the binary events, which is expressed as

$$T_h^{i,beg} = \sum_{t\in\mathcal{T}} t \bullet N_{h,t}^{i} \quad \forall i \in \{DRI,Tr / EAF / LF / CC / HR\} \quad (25)$$

$$T_h^{i,end} = \sum_{t\in\mathcal{T}} t \bullet N_{h,t}^{i,end} \quad \forall i \in \{EAF / LF / CC / HR\} \quad (26)$$

E. Adjustable Power for EAF & LF

During operation, the EAF and LF power setpoints are constrained by up/down ramp-rate limits, which is expressed as

$$P_{h,t}^{i} - P_{h,t-1}^{i} \leq \overline{P^{i,\uparrow}} \bullet S_{h,t-1}^{i} + \overline{P^{i}} \bullet N_{h,t}^{i} \quad \forall i \in \{EAF / LF\} \quad (27)$$

$$P_{h,t-1}^{i} - P_{h,t}^{i} \leq \overline{P^{i,\downarrow}} \bullet S_{h,t}^{i} + \overline{P^{i}} \bullet N_{h,t}^{i,end} \quad \forall i \in \{EAF / LF\} \quad (28)$$

For each EAF heat, the required processing energy is provided by a combination of electricity and CO. For LF, the requirement is supplied solely by electricity, which is expressed as

$$\delta \bullet \sum_{t\in\mathcal{T}} P_{h,t}^{EAF} + K^{CO} \bullet \sum_{t\in\mathcal{T}} \xi_{h,t}^{CO,EAF,c} = E^{EAF,c} \quad (29)$$

$$\delta \bullet \sum_{t\in T} P_{h,t}^{LF} = E^{LF,c} \quad (30)$$

III. Flexibility Evaluation Method

A. Characterization of Flexibility

The flexibility evaluation is based on the production baseline, defined as the schedule that minimizes total electricity cost for the short-process steelmaking system, which is expressed as

$$C = \min \ \pi_t \bullet \sum_i \sum_{h\in\mathcal{H}} P_{h,t}^i \quad \forall i \in \{EAF / LFCC / HR\} \tag{31}$$

where π_t denotes the electricity price at time slot *t*.

As shown in Fig. 3, flexibility $\mathcal{F}$ is decomposed into valley-filling capacity $F^{\uparrow}$ and peak-shaving capacity $F^{\downarrow}$. The valley-filling capacity is the minimum increase above the production baseline across all grid-required averaging intervals within the service window; the peak-shaving capacity is the minimum decrease below the baseline across the same intervals, which is expressed as

$$\mathcal{F} = \begin{cases} F^{\uparrow} = \min\limits_{t\in W} \left[\sum\limits_i \sum\limits_{h\in\mathcal{H}} P_{h,t}^i - \sum\limits_i \sum\limits_{h\in\mathcal{H}} P_{h,t}^{i,baseline} \right] \\ F^{\downarrow} = \min\limits_{t\in W} \left[\sum\limits_i \sum\limits_{h\in\mathcal{H}} P_{h,t}^{i,baseline} - \sum\limits_i \sum\limits_{h\in\mathcal{H}} P_{h,t}^i \right] \end{cases} \tag{32}$$

$$\forall i \in \{EAF / LF / CC / HR\}$$

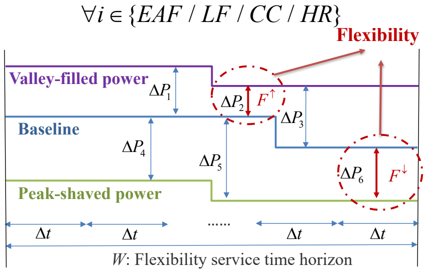

Fig. 3. Definition of flexibility over the service window.

When a flexibility requirement is specified, the schedule is obtained by minimizing (31) subject to the following additional constraint. The objective increase relative to the baseline schedule quantifies the additional electricity cost.

$$F^{\uparrow} \ge F_{req}^{\uparrow} \text{ (valley filling) or } F^{\downarrow} \ge F_{req}^{\downarrow} \text{ (peak shaving)} \tag{33}$$

B. Resource Bounds of the Flexibility Evaluation

In a short-process steelmaking system, flexibility is bounded by material storage capacities, equipment capacities (including production units and transfer cars), and the power envelopes of the adjustable units (EAF and LF).

At all times, the material-storage resources are constrained by their capacity limits, which is expressed as

$$\underline{R^{i,sto}} \le R_t^{i,sto} \le \overline{R^{i,sto}} \quad \forall i \in \{H_2 / CO / DRI\} \tag{34}$$

At the CC ladle turret, at most one heat may be present at any time, which is expressed as

$$\sum_{h\in\mathcal{H}} S_{h,t}^{CC,arr} \le 1 \tag{35}$$

At all times, production equipment resources are constrained by their capacity limits, which is expressed as

$$\underline{R^i} \le R_t^i \le \overline{R^i} \quad \forall i \in \{EAF / LF / CC / HR\} \tag{36}$$

At all times, the transfer-car resources are constrained by their capacity limits, which is expressed as

$$\underline{R^{i,Car}} \le R_t^{i,Car} \le \overline{R^{i,Car}} \quad \forall i \in \{DRI / EAF / LF\} \tag{37}$$

During production, the EAF and LF have adjustable power bounded by lower and upper limits, which is expressed as

$$S_{h,t}^i \bullet \underline{P^i} \le P_{h,t}^i \le S_{h,t}^i \bullet \overline{P^i} \quad \forall i \in \{EAF / LF\} \tag{38}$$

IV. Case Study

A. Case Description

The evaluation method is tested with data from a real steel plant featuring 2 EAFs, 2 LFs, 1 CC, and 2 HR, and the main parameters are given in TABLE I. The test case includes 20 heats arranged as four casting sequences of five heats each. The grid-required averaging interval is 15 min, while the model uses 5-min slots.

TABLE I. Equipment Parameters

Process	Power range	Key model parameters
EAF	40-80 MW	$\overline{P^{\uparrow}}$ / $\overline{P^{\downarrow}}$ =1.5/2.0 MW/min, $E^{EAF,c}$ =50 MWh
LF	15-25 MW	$\overline{P^{\uparrow}}$ / $\overline{P^{\downarrow}}$ =1.0/1.0 MW/min, $E^{LF,c}$ =10 MWh
CC	8 MW	casting time=30 min/heat, T_{fix}^{chg} =45 min
HR	25 MW	rolling time=30 min/heat

B. Baseline Schedule and Flexibility Results

Baseline load and time-of-use (TOU) electricity price [14] are shown in Fig. 4 (a), and the baseline batch schedules of EAF, LF, CC, and HR are shown in Fig. 4 (b). To minimize electricity cost, total load and EAF/LF operation are concentrated in valley periods. In the first peak period, only fixed, low-power stages (CC and HR) are active; in the second peak period, the EAF and LF operate at low power. The overall schedule is constrained by the CC casting sequence.

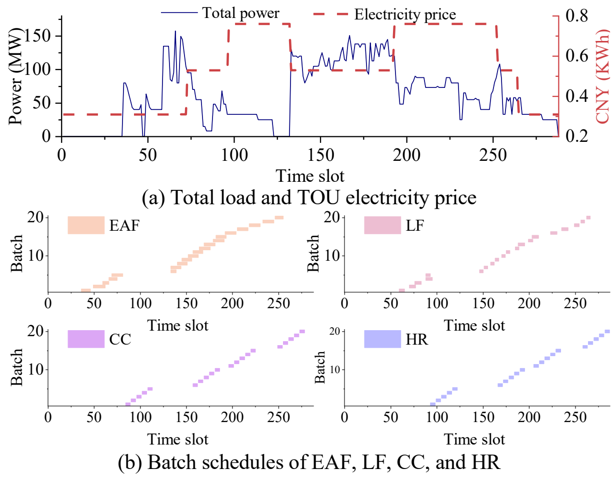

Fig. 4. Baseline production and load.

As shown in Fig. 5, driven by the PV diurnal cycle, H₂ and CO production from the PV-EC system varies over the day. Early-day H₂ demand is met from initial inventory, with subsequent surpluses stored. CO use is dominated by HR and follows the batch schedule, while the CO supplied to the EAF is capped and coincides with its melting periods. Thus, while the PV profile shapes the time-varying availability of H₂ and CO, the inventories buffer the short-process plant from early-hour PV scarcity and smooth the impact of PV variability on batch scheduling.

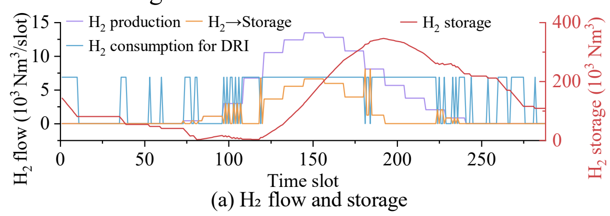

979-8-3315-8138-1

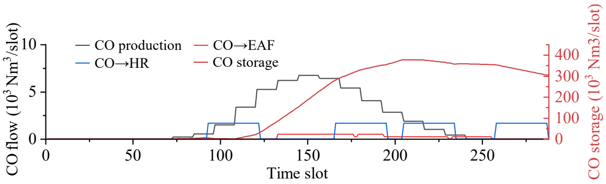

(b) CO flow and storage

Fig. 5. H_2/CO flow and storage under the baseline schedule.

As shown in Fig. 6, flexibility depends strongly on the signal start time. In Fig. 6 (a), peak-shaving is higher with H_2/CO coupling than that under the conventional H_2-only flexibility evaluation method. Valley-filling capacity is greatest during CC changeover intervals, whereas peak-shaving capacity is highest in production-intensive periods. In addition, increasing the service duration depresses the deliverable flexibility, since it is defined by the minimum sustainable power differential over the entire window. These flexibility envelopes can support scheduling of the plant under system-level PV variability.

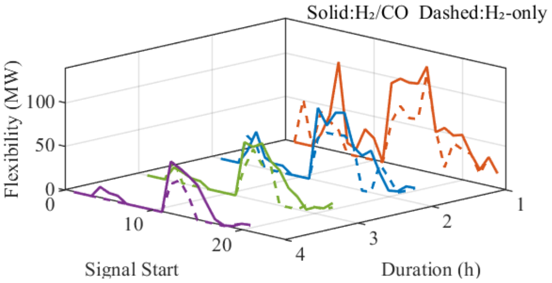

(a) Peak-shaving capability (H_2/CO vs H_2-only)

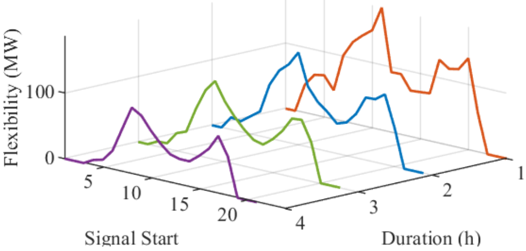

(b) Valley-filling capability

Fig. 6. Flexibility evaluation results under various service durations.

Fig. 7 shows the schedule that minimizes electricity cost subject to a 60-MW peak-shaving constraint, together with the baseline schedule for comparison. Within the service window, overlapping heats are reduced and both the EAF and LF run near the lower bounds of their power envelopes. Outside the window, load is preferentially shifted to valley periods to reduce electricity cost; however, the finite number of heats and sequencing constraints still push a substantial share of production into peak-price periods, which increases the daily electricity cost by 6.32% relative to the baseline (from 793,986.15 to 844,183.65).

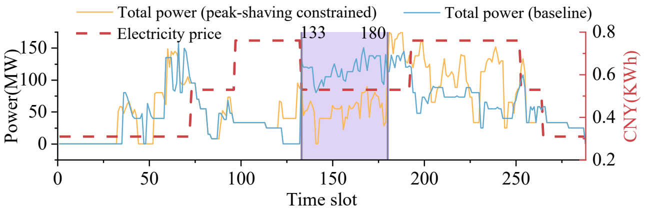

Fig. 7. Maximum peak-shaving capacity at minimum cost with 4-h service starting at signal 12.

V. Conclusion

This paper proposes a plant-level flexibility evaluation method for PV-EC-integrated hydrogen-based DRI short-process steel plants. The method is formulated using a batch-oriented RTN model of the integrated plant to evaluate its peak-shaving and valley-filling capability. Case studies show that PV-driven H_2/CO production shapes feasible production schedules. H_2/CO storage mitigates temporal mismatches between PV output and steelmaking demand and thereby supports flexibility provision. Flexibility is strongly affected by batch-scheduling windows. Production-intensive periods and CC changeover intervals provide the largest flexibility margins. For a given start time, the available capacity tends to decrease as the service duration increases. In the studied case, providing flexibility requires shifting heats into higher-price periods and thus raises the total electricity cost, illustrating a trade-off between flexibility and operating cost.

References

[1] M. J. Fell, "Just flexibility?," Nature Energy, vol. 5, no. 1, pp. 6-7, Dec. 2019.

[2] R. Wang, J. Ma, H. Sheng, V. M. Zavala, and S. Jin, "Exploiting different electricity markets via highly rate-mismatched modular electrochemical synthesis," Nature Energy, vol. 9, pp. 1064-1073, Jul. 2024.

[3] M. Paulus and F. Borggrefe, "The potential of demand-side management in energy-intensive industries for electricity markets in Germany," Applied Energy, vol. 88, no. 2, pp. 432-441, Feb. 2011.

[4] W. Sun, Q. Wang, Y. Zhou, and J. Wu, "Material and energy flows of the iron and steel industry: Status quo, challenges and perspectives," Applied Energy, vol. 268, p. 114946, Jun. 2020.

[5] L. Ge et al., "Electrochemical CO2 reduction in membrane-electrode assemblies," Chem, vol. 8, no. 3, pp. 663-692, Mar. 2022.

[6] N. Torres, G. Greivel, J. Betz, E. Moreno, A. Newman, and B. Thomas, "Optimizing steel coil production schedules under continuous casting and hot rolling," European Journal of Operational Research, vol. 314, no. 2, pp. 496-508, Apr. 2024.

[7] T. A. C. Maia and V. C. Onofri, "Survey on the electric arc furnace and ladle furnace electric system," Ironmaking & Steelmaking, vol. 49, no. 10, pp. 976-994, Oct. 2022.

[8] P. M. Castro, L. Sun, and I. Harjunkoski, "Resource-task network formulations for industrial demand side management of a steel plant," Industrial & Engineering Chemistry Research, vol. 52, no. 36, pp. 13046-13058, Aug. 2013.

[9] X. Zhang, G. Hug, and I. Harjunkoski, "Cost-effective scheduling of steel plants with flexible EAFs," IEEE Trans. Smart Grid, vol. 8, no. 1, pp. 239-249, Jan. 2017.

[10] J. Wang, Q. Wang, and W. Sun, "Optimal power system flexibility-based scheduling in iron and steel production: A case of steelmaking-refining-continuous casting process," Journal of Cleaner Production, vol. 414, pp. 137619-137619, May. 2023.

[11] J. Wang, Q. Wang, and W. Sun, "Quantifying flexibility provisions of the ladle furnace refining process as cuttable loads in the iron and steel industry," Applied Energy, vol. 342, pp. 121178-121178, Jul. 2023.

[12] T. Li and Z. Lv, "A novel two-stage method for collaboratively scheduling of steel production and energy in steelmaking and continuous casting processes," in Proc. ICIEA, Tokyo, Japan, 2019, pp. 54-58.

[13] P. Su, Y. Zhou, H. Li, H. D. Perez, and J. Wu, "Cost-effective scheduling of a hydrogen-based iron and steel plant powered by a grid-assisted renewable energy system," Applied Energy, vol. 384, p. 125412, Feb. 2025.

[14] X. Zhao, H. Bai, Q. Shi, X. Lu, and Z. Zhang, "Optimal scheduling of a byproduct gas system in a steel plant considering time-of-use electricity pricing," Applied Energy, vol. 195, pp. 100-113, Jun. 2017.

979-8-3315-8138-1